JOURNAL OF SPACECRAFT AND ROCKETS
Vol. 46, No. 6, November–December 2009

Coning Control of Solar Sails Using Magnetic Momentum Error Reduction

Dale A. Lawrence*
University of Colorado, Boulder, Colorado 80309
and
Mark S. Whorton†
Teledyne Brown Engineering, Huntsville, Alabama 35805

DOI: 10.2514/1.43088

Magnetic attitude control of a solar sail is investigated for orbit rate coning of the sail normal in low Earth orbits. Coning is found to provide significant solar thrust effects on orbit parameters but with smooth torque that minimizes excitation of low frequency modes in the sail structure. By spinning the sail about its normal at specific rates, coning is achieved with zero control torque, enabling asymptotic stabilization of these equilibria in the local-vertical–local-horizontal frame despite the underactuation inherent in magnetic control. Lyapunov stability properties of these equilibria are determined under specific types of magnetic control, including a new angular momentum error reduction control law. Performance of a 3 kg CubeSat class microsailcraft is examined under magnetic coning control, showing that reliable convergence to equilibria in local-vertical–local-horizontal occurs, even in some naturally unstable cases, but that magnetic stabilization of other unstable equilibria is tenuous.

Nomenclature

A	=	planet-centered inertial frame ($\hat{x}$, $\hat{y}$, $\hat{z}$)
A_s	=	sail area, m^2
a	=	orbit semimajor axis, m
B	=	intermediate sailcraft-centered frame ($\hat{l}$, $\hat{m}$, $\hat{n}$)
$\boldsymbol{B}$	=	Earth magnetic flux density vector, Wb/m^2
C	=	sailcraft body-fixed frame ($\hat{p}$, $\hat{q}$, $\hat{n}$)
C_D	=	ballistic coefficient of drag
f_s	=	specular reflectance fraction
${}^A\mathbf{h}_C$	=	inertial angular momentum vector of C about the sailcraft center of the mass, $N \cdot m \cdot s$
${}^A\mathbf{h}_{Co}$	=	desired angular momentum vector, $N \cdot m \cdot s$
$\mathbf{I}$	=	identity tensor
I_n, and I_T	=	principal sailcraft moments of inertia about/transverse to the sail normal, $kg \cdot m^2$
$\mathbf{I}_s$	=	sailcraft moment of inertia tensor about the sailcraft center of mass, $kg \cdot m^2$
k, k_d, and k_s	=	control gains, $N \cdot m \cdot s/rad$
L	=	local-vertical–local-horizontal orbit frame ($\hat{r}$, $\hat{v}$, $\hat{o}$)
$\boldsymbol{M}_c$	=	control magnetic moment, $A \cdot m^2$
P	=	solar pressure, N/m^2
r_c	=	sailcraft center-of-pressure to center-of-mass offset, m
V_1, V_h	=	Lyapunov functions
v	=	sailcraft velocity relative to the atmosphere, m/s
β and ϕ	=	cone and clock angles of the sail normal $\hat{n}$ in L, rad
μ	=	planetary gravitational constant, m^3/s^2
ρ	=	atmospheric density, kg/m^3
τ_{am}, τ_{sm}, and τ_{gm}	=	moment coefficient due to aerodynamic, solar, and gravity gradient torque, $N \cdot m$
τ_c and τ_e	=	control and environmental torques, $N \cdot m$
Ψ_a, Ψ_s, and Ψ_g	=	aerodynamic, solar, and gravity gradient potentials, $N \cdot m/rad$
${}^A\boldsymbol{\omega}_C$	=	angular velocity vector of C as seen in A, rad/s
ω_n	=	component of ${}^A\boldsymbol{\omega}_C$ along the sail normal $\hat{n}$
ω_{no}	=	equilibrium value of ω_n
ω_o	=	orbit angular velocity, rad/s
ω_r, ω_{sr}	=	relative angular velocities, rad/s
ω_T	=	component of ${}^A\boldsymbol{\omega}_B$ orthogonal to $\hat{n}$
$\omega_\perp$	=	component of ${}^A\boldsymbol{\omega}_L$ along $\hat{n}$

Introduction

IN SOLAR sailing, thrust is obtained by pointing the sail normal vector $\hat{n}$ at particular orientations relative to the spacecraft–sun vector $\hat{s}$. For example, in planetary orbits, coning of the sail normal at orbit rates can produce a component of solar thrust that remains aligned with the spacecraft orbit velocity vector. This provides a consistent delta-v that can raise or lower the orbit semimajor axis without expendable propellant. For example, a perfectly reflective 40 m^2 sail at 1 astronomical unit (AU) from the sun produces a maximum solar radiation thrust of approximately 3.6×10^{-4} N. With a 3 kg microsailcraft, this produces a maximum acceleration of 0.12 mm/s^2. Orienting the sail at a cone angle of $\beta = 30$ deg relative to the sun produces a solar delta-v along the orbit velocity direction of about 0.3 m/s per orbit at 1000 km altitude, resulting in an increase in semimajor axis of about 0.6 km per orbit, or about 8 km per day.

For interplanetary trajectories, coning of the sail normal can be used to modulate solar thrust magnitude (e.g., for continuous trajectory correction [1]). Coning may be an attractive alternative to dithering or orbiting [2] methods, because coning can be accomplished with zero torque [3] if the sailcraft is spun about its normal at the proper rate.

In planetary orbits, zero control torque coning is desirable because the environmental torques are significant for solar sails. Sailcraft are designed to maximize area-to-mass ratio for the highest lightness factor [4] (or acceleration), resulting in greatly magnified forces due to solar radiation pressure (desired) and aerodynamic drag (undesired).

Presented as Paper 7161 at the Guidance, Navigation, and Control Conference, Honolulu, HI, 18–21 August 2008; received 05 January 2009; revision received 05 August 2009; accepted for publication 11 August 2009.

*Associate Professor, Aerospace Engineering Sciences; dale.lawrence@colorado.edu. Associate Fellow AIAA.

†Director, Systems Development and Operations Support; mark.whorton@tbe.com. Associate Fellow AIAA.

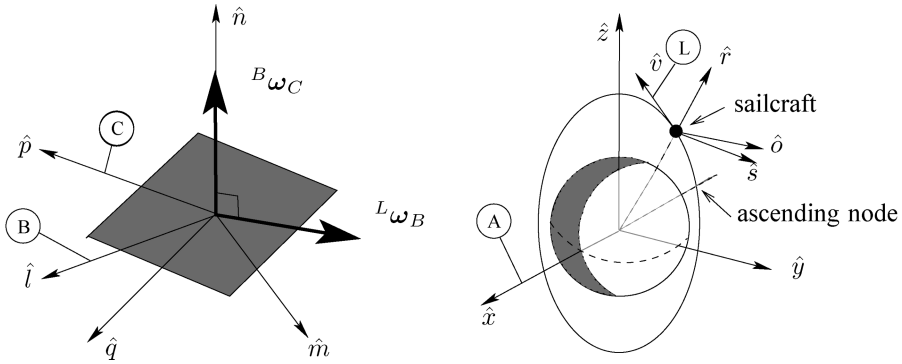

Fig. 1 Reference frames used to develop sailcraft dynamics and performance simulations.

Resulting environmental torques are therefore very sensitive to the center-of-pressure (CP) to center-of-mass (CM) offset, which is difficult to predict due to uncertainties in the gossamer structure deployed shape [5] and shape changes due to solar and aerodynamic pressure loading [6–8]. Although solar torques are usually considered in attitude control, these have been among the smallest disturbances in conventional spacecraft and typically do not drive the design of either the control actuators or the algorithms. The large sailcraft area also tends to push mass properties toward that of a flat plate, resulting in significant gravity gradient torques.

Three-axis control in the presence of large environmental disturbances requires correspondingly large control torques, unless the mission design allows operation at attitudes near nulls in the environmental torques. The same is true for conventional spin stabilization; larger angular momentum slows the rate of precession, but disturbances must still be countered if long-term pointing is required. Unfortunately, large control torques require sophisticated and massive actuation (e.g., reaction wheels or control moment gyros and life-limiting reaction jets). The resulting burdens on spacecraft mass and cost would make a conventional approach inappropriate for small sailcraft programs or long-duration missions.

In low Earth orbit, magnetic control torque is attractive because it is simple to actuate using electric current in orthogonal torque rods or coils, hence it is low cost, low mass, and requires no expendables. Unfortunately, available torque is small and, most important, is restricted in direction to be orthogonal to the local magnetic field vector. As this direction is a function of orbit position, successful attitude control cannot be guaranteed in general. In this paper, we show that magnetic attitude control can be obtained by using the conservative environmental torques together with spinning spacecraft dynamics to produce neutrally stable equilibria. The main idea [3,9] is to spin the sailcraft at a specific rate so that environmental torques provide desired precession of the momentum vector to maintain a desired inertial coning of the sail normal. The spin rates are on the order of orbit rate, hence are small compared with conventional spin stabilization of solar sails for inertial pointing [7,10,11]. The resulting equilibria are similar to the classical Likins–Pringle equilibria [12] due to gravity gradients, except that the effects of solar and aerodynamic environmental torques are also incorporated. In this paper, we show these equilibria can be made asymptotically stable by a variation of the classical B-dot magnetic damping law. We also show that stabilizing potentials can be obtained from magnetic torque in some cases using a new Lyapunov technique based on the reduction of angular momentum error. This allows operation at other equilibria that are naturally unstable.

The first section of this paper summarizes fundamental dynamics of a spinning solar sail in Earth orbit and the resulting equilibrium and stability conditions from earlier work [9]. The next section builds on this foundation, providing a Lyapunov stability analysis of a relative B-dot damping law and a new magnetic momentum error reduction control approach. The last section provides detailed simulation evaluations of these control laws in several mission operational modes of a 3 kg microsailcraft designed to deploy from a 3U CubeSat envelope.

Sailcraft Dynamics

Reference Frames

Key reference frames are the Earth-centered inertial frame $A = (\hat{x}, \hat{y}, \hat{z})$ with $\hat{x}$ and $\hat{y}$ in the equatorial plane, $\hat{z}$ normal to the equatorial plane, and $\hat{x}$ along the vernal equinox. $L = (\hat{r}, \hat{v}, \hat{o})$ is the local-vertical–local-horizontal (LVLH) frame, with $\hat{r}$ in the orbit radial direction, $\hat{v}$ along the sailcraft velocity vector, and $\hat{o}$ aligned with the orbit angular momentum. $C = (\hat{p}, \hat{q}, \hat{n})$ is the sailcraft body-fixed frame, with $\hat{n}$ normal to the plane of the sail, and $\hat{p}$ and $\hat{q}$ fixed in the plane of the sail. Frame $B = (\hat{l}, \hat{m}, \hat{n})$ differs from C only in rotation about $\hat{n}$, to be described next. Figure 1 illustrates these frames.

Equations of Motion

The sailcraft will be assumed to be a rigid body with a uniform, flat, square sail, and a sailcraft CM located a distance of r_c along $\hat{n}$, due to portions of the spacecraft bus located out of the sail plane. The CP–CM offset r_c scales the aerodynamic and solar environmental torques. The sailcraft moment of inertia tensor $\mathbf{I}_s$ has principal axes $(\hat{p}, \hat{q}, \hat{n})$, and due to the symmetry about $\hat{n}$, the frame B is also a principal frame.[‡] Let I_n be the principal moment of inertia about $\hat{n}$ and I_T be the principal moment of inertia about any transverse principal axis. Typically, the bus is located near the plane of the sail, making the overall inertia tensor similar to that of a flat plate [13], so that $I_n \approx 2I_T$.

Although a sailcraft will be nonrigid by conventional spacecraft standards, the orbit element control application, using coning motions, produces very smooth low-frequency environmental torques on the order of orbit frequency and only requires closed-loop settling times on the order of several orbits. In contrast, attitude stability of a flexible solar sail with much faster settling times can be problematic [14]. Here, the disturbance frequencies and control system bandwidths are on the order of 10^{-4} Hz, whereas the lowest structural sail modes are likely [8,15] to be in the range of 10^{-1} to 10^{-2} Hz, justifying the rigid-body treatment from a control-structure interaction viewpoint. Quasi-static effects of sail deformation due to pressure loading are also important in attitude dynamics because they cause the CP–CM of the sailcraft to vary with attitude [6,8]. As these are secondary effects on sailcraft torque as a function of attitude, the analysis here focuses on the ideal (flat) case.

Dynamics are derived [9] from the relation between the inertial angular momentum vector ${}^{A}\mathbf{h}_{C}$ of the body (frame C) and the inertial angular velocity vector ${}^{A}\boldsymbol{\omega}_{C}$. With the net external moment (torque) vector on the body given by $\boldsymbol{\tau}$, we have

$$\boldsymbol{\tau} = \mathbf{I}_s \cdot \frac{{}^{B}\mathrm{d}}{\mathrm{d}t}{}^{A}\boldsymbol{\omega}_{C} + {}^{A}\boldsymbol{\omega}_{B} \times (\mathbf{I}_s \cdot {}^{A}\boldsymbol{\omega}_{C}) \tag{1}$$

where we have defined frame B such that the relative velocity ${}^{L}\boldsymbol{\omega}_{B}$ of B as seen in L is zero along $\hat{n}$, so that B describes the tip and tilt of the sailcraft normal $\hat{n}$ with respect to the LVLH frame L. The additional

[‡]Note that a square sail and a disk sail have the same invariance of the inertia matrix for coordinate rotation about the sail normal.

sailcraft spin about $\hat{n}$, relative to L, is purposefully not included in B, because this does not affect the force vector produced by the sail (due to sail symmetry about $\hat{n}$). This symmetry also implies that $\mathbf{I}_s$ is fixed in B. We have the inertial spin about $\hat{n}$ given by

$$\omega_n = \hat{n} \cdot {}^A\boldsymbol{\omega}_C = \hat{n} \cdot ({}^A\boldsymbol{\omega}_L + {}^L\boldsymbol{\omega}_B + {}^B\boldsymbol{\omega}_C) \tag{2}$$

Taking advantage of the symmetric mass properties by partitioning ${}^A\boldsymbol{\omega}_B = (I - \hat{n}\,\hat{n}) \cdot {}^A\boldsymbol{\omega}_B + (\hat{n}\,\hat{n}) \cdot {}^A\boldsymbol{\omega}_B$, we define the first term (normal to $\hat{n}$) as $\boldsymbol{\omega}_T$ and note that the second term is equal to $\omega_o(\hat{o} \cdot \hat{n})\hat{n}$. Then

$$\mathbf{I}_s \cdot {}^A\boldsymbol{\omega}_C = \mathbf{I}_s \cdot {}^A\boldsymbol{\omega}_B + I_n\omega_s\hat{n} = I_T\boldsymbol{\omega}_T + I_n\omega_n\hat{n} \tag{3}$$

This enables the dynamics to be written in terms of transverse (orthogonal to $\hat{n}$) and normal (along $\hat{n}$) components:

$$\boldsymbol{\tau}_T = I_T \frac{{}^B\mathrm{d}}{\mathrm{d}t}\boldsymbol{\omega}_T + [\omega_n I_n - \omega_o(\hat{o} \cdot \hat{n})I_T]\boldsymbol{\omega}_T \times \hat{n} \tag{4}$$

$$\tau_n = I_n\dot{\omega}_n \tag{5}$$

Precession Equilibria

Suppose $\hat{n}$ is fixed in L, then B is also fixed in L by definition of the B frame (${}^L\boldsymbol{\omega}_B \cdot \hat{n} = 0$). Then ${}^L\boldsymbol{\omega}_B = 0$ and ${}^A\boldsymbol{\omega}_C = {}^A\boldsymbol{\omega}_L + {}^B\boldsymbol{\omega}_C$, so that

$$\frac{{}^B\mathrm{d}}{\mathrm{d}t}{}^A\boldsymbol{\omega}_C = \frac{{}^L\mathrm{d}}{\mathrm{d}t}({}^A\boldsymbol{\omega}_L + {}^B\boldsymbol{\omega}_C) = 0 \tag{6}$$

where the last equality comes from the assumption that ω_o is constant (a reasonable assumption because sail forces change the semimajor axis, and hence the orbit period, slowly when compared with the orbit rate and the sail attitude motions), and from the assumption that the torque along $\hat{n}$ is zero, which [from Eq. (5)] implies that ω_n is constant. Using Eq. (6) in Eq. (1), at an equilibrium in L, Eq. (4) becomes

$$\boldsymbol{\tau}_T = [\omega_n I_n - \omega_o(\hat{o} \cdot \hat{n})I_T]\boldsymbol{\omega}_T \times \hat{n} \tag{7}$$

We write the right-hand side of Eq. (7) in L coordinates, using a cone angle β and a clock angle ϕ, as shown in Fig. 2. Then

$$\hat{n} = -(\sin\beta\sin\phi)\hat{r} + (\sin\beta\cos\phi)\hat{v} + (\cos\beta)\hat{o} \tag{8}$$

and the equilibrium condition Eq. (7) becomes [9]

$$\boldsymbol{\tau}_T = -(\omega_n I_n - \omega_o I_T\cos\beta)\omega_o\sin\beta(\cos\phi\hat{r} + \sin\phi\hat{v}) \tag{9}$$

Environmental Torques

The aerodynamic torques $\boldsymbol{\tau}_a$ on the sailcraft depend [12,16] on the orientation of the sail normal $\hat{n}$ relative to the aerodynamic force vector, which is approximately[§] directed along the sailcraft velocity vector $\hat{v}$, resulting in

$$\boldsymbol{\tau}_a = -\tau_{\mathrm{am}}|\hat{v} \cdot \hat{n}|\hat{v} \times \hat{n} = -\tau_{\mathrm{am}}\sin\beta|\cos\phi|(\cos\beta\hat{r} + \sin\beta\sin\phi\hat{o}) \tag{10}$$

where $\tau_{\mathrm{am}} = 1/2r_c\rho C_D v^2 A_s \geq 0$ is the aerodynamic moment coefficient. (Note that $\beta \in [0, \pi]$, because aerodynamic forces impinge equally on either the front or the back of the sail).

Similarly, solar torque $\boldsymbol{\tau}_s$ depends [12,16] on the orientation of $\hat{n}$ relative to the sailcraft-to-sun vector $\hat{s}$:

$$\boldsymbol{\tau}_s = -\tau_{\mathrm{sm}}|\hat{s} \cdot \hat{n}|\hat{s} \times \hat{n} = \tau_{\mathrm{sm}}\sin\beta|\cos\beta|(\cos\phi\hat{r} + \sin\phi\hat{v}) \tag{11}$$

where $\tau_{\mathrm{sm}} = r_c(1 - f_s)PA_s \geq 0$ is the solar moment coefficient, and assuming that the orbit is normal to the sun (i.e., $\hat{s} = \hat{o}$). More complex models can be used [4,5] for the optical properties, although the simple model captures the principal effects. Orbit–sun vector misalignment can be a significant effect and is treated as a perturbation in the Magnetic Control Robustness section.

Gravity gradient torques $\boldsymbol{\tau}_g$ are given by [12,16]

$$\boldsymbol{\tau}_g = \frac{3\mu}{a^3}[\hat{r} \times (\mathbf{I}_s \cdot \hat{r})] = 3\tau_{\mathrm{gm}}\sin\beta\sin\phi(\cos\beta\hat{v} - \sin\beta\cos\phi\hat{o}) \tag{12}$$

where we have used $\mathbf{I}_s = I_n\hat{n}\,\hat{n} + I_T(\mathbf{I} - \hat{n}\,\hat{n}) = (I_n - I_T)\hat{n}\,\hat{n} + I_T\mathbf{I}$, $\omega_o = \sqrt{\mu/a^3}$, and Eq. (8). Note that the gravity moment coefficient $\tau_{\mathrm{gm}} = \omega_o^2(I_n - I_T) \geq 0$ depends on sailcraft mass properties and orbit radius.

Equilibrium Spin

For the net torque $\boldsymbol{\tau} = \boldsymbol{\tau}_a + \boldsymbol{\tau}_s + \boldsymbol{\tau}_g$ to satisfy Eq. (9), we have three simultaneous equations from the three vector components, with inertial spin ω_n free to choose. A given cone β and a clock ϕ angle orientation of $\hat{n}$ in L is an equilibrium solution to the attitude dynamics if a nominal spin rate $\omega_n = \omega_{\mathrm{no}}$ exists to satisfy these three equations for arbitrary values of τ_{am}, τ_{sm}, I_n, I_T, and ω_o. Cases in which equilibrium occurs due to particular relationships between these parameters are excluded, because this would require specific orbit and sailcraft properties that would be unlikely to occur in practice. When the sun $\hat{s}$ is aligned with the orbit normal $\hat{o}$, the complete set of equilibria are classified as follows.

For type I equilibria, $\sin\beta = 0$. Then, $\hat{n}$ is inertially pointed, and there is no coning. This corresponds to conventional spin stabilization with the inertial spin rate ω_{no}. All three constraints are satisfied for any ϕ and any ω_{no}. When $\beta = 0$, designated as type I.A, we have orbit-normal pointing. When $\beta = \pi$, the equilibrium is designated as type I.B, and we have anti-orbit-normal pointing of the sail normal vector.

For type II equilibria, $\cos\beta = 0$. Here, $\hat{n}$ lies in the plane of the orbit, and the sail is edge-on to the sun (no solar thrust), rotating in the inertial frame about an axis in the plane of the sail at orbit rate. This requires $\omega_{\mathrm{no}} = 0$ and $\cos\phi\sin\phi = 0$. When $\sin\phi = 0$ (type II.A), we have velocity (type II.A.1) or antivelocity (type II.A.2) pointing. This provides maximum aerodynamic drag that can be used to minimize the deorbit time, mitigating orbital debris concerns. When $\cos\phi = 0$ (type II.B), we have nadir or antinadir pointing. This may be useful for viewing the deployed sail shape from ground telescopes.

For type III equilibria, $\cos\beta\sin\beta \neq 0$. This requires $\cos\phi\sin\phi = 0$. The sail normal cones in the inertial frame at orbit rate, and solar thrust is produced. When $\sin\phi = 0$, the equilibria are designated as type III.A. For $\phi = 0$ (type III.A.1), a component of the solar thrust vector lies in the antivelocity direction, reducing orbit energy, hence reducing the orbit semimajor axis a. This requires the equilibrium spin rate:

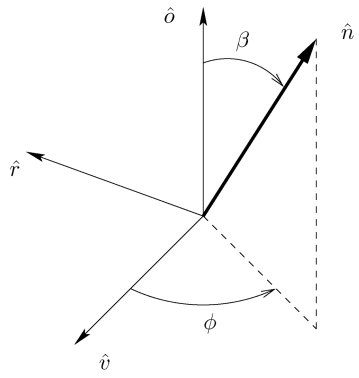

Fig. 2 Cone and clock angles of the sail normal $\hat{n}$ relative to the LVLH frame L.

[§]Because the atmosphere rotates with the Earth, there is a sinusoidal component of aerodynamic force in the $\hat{o}$ direction (with orbit period), but this is approximately a factor of 15 smaller than the principal $\hat{v}$ component modeled here.

$$\omega_{\rm no} = \frac{\cos\beta}{I_n \omega_o}[\omega_o^2 I_T + \tau_{\rm am} - \tau_{\rm sm}\,\text{sign}\,(\cos\beta)] \tag{13}$$

For $\phi = \pi$ (type III.A.2), a component of solar thrust lies in the velocity direction, increasing orbit energy and a over time. This requires a spin rate:

$$\omega_{\rm no} = \frac{\cos\beta}{I_n \omega_o}[\omega_o^2 I_T - \tau_{\rm am} - \tau_{\rm sm}\,\text{sign}\,(\cos\beta)] \tag{14}$$

When $\cos\phi = 0$, the equilibrium is type III.B. This produces a component of solar thrust in the radial or antiradial directions. The required spin rate is

$$\omega_{\rm no} = \frac{\cos\beta}{I_n \omega_o}[\omega_o^2 I_T - 3\tau_{\rm gm} - \tau_{\rm sm}\,\text{sign}\,(\cos\beta)] \tag{15}$$

The complete set of equilibria is shown in Fig. 3.

Orbit and sailcraft design choices affect the parameters $\tau_{\rm am}$, $\tau_{\rm sm}$, and $\tau_{\rm gm}$, influencing the set of feasible equilibria. The CP–CM offset on the sailcraft scales $\tau_{\rm am}$ and $\tau_{\rm sm}$, relative to $\tau_{\rm gm}$. The case of zero CP–CM offset was treated in [3], in which gravity gradient torque $3\tau_{gm}$ was also assumed to be zero (approximated by a sailcraft in a solar orbit where ω_o was very small). This produces $\tau_{\rm am} = \tau_{\rm sm} = 0$ and the $3\tau_{\rm gm}$ gravity gradient term disappears from (15), leaving the two type I equilibria and (possibly, depending on $\omega_{\rm no}$) a single other equilibrium satisfying

$$\omega_{\rm no} = \frac{\cos\beta}{I_n \omega_o}\omega_o^2 I_T = \omega_o \cos\beta \frac{I_T}{I_n} \tag{16}$$

where ω_o, in this case, is the desired coning rate of the sail normal and not the orbit rate.

For circular planetary orbits with 0 CP–CM offset, the gravity gradient torque $3\tau_{\rm gm}$ reappears in Eq. (15), but $\tau_{\rm am}$ and $\tau_{\rm sm}$ remain zero in Eqs. (13–15). The type I equilibria in this case were first analyzed by Thomson [17]. Types III.A.1 and III.A.2 equilibria have the same conditions as Eq. (16), but type III.B equilibria are distinguished by a different $\omega_{\rm no}$. These zero CP–CM equilibria are also well known in this case, and are referred to as Likins–Pringle equilibria [18,19], with type III.A denoted as hyperbolic because the spin axis appears to trace out a hyperboloid in inertial space as the spin axis moves with the spacecraft along the orbit. Similarly, type III.B has been denoted as conical due to the set described by the spin axis in A along the orbit. Both are described here as coning in A, because the spin axis traces out a cone in A when A remains centered at the sailcraft CM.

When the CP–CM offset is nonzero, but the orbit is high relative to the planet's atmosphere, $\tau_{\rm sm}$ becomes nonzero in the type III equilibrium conditions. This produces additional equilibria, owing to the $|\cos\beta|$ dependence in the solar torque. If the CP–CM offset and sail area are small enough, $\tau_{\rm sm} < \omega_o^2 I_T$ and type III.A equilibria exist with both prograde and retrograde inertial spin $\omega_{\rm no}$, with respect to ω_o. Otherwise, $\omega_{\rm no}$ is nonpositive (retrograde). Similarly, $\omega_{\rm no}$ has both signs for type III.B equilibria when $\tau_{\rm sm} < \omega_o^2 I_T - 3\tau_{\rm gm}$, and $\omega_{\rm no}$ is nonpositive otherwise.

For lower orbits, atmospheric torques become significant, and the $\tau_{\rm am}$ terms in the type III.A equilibrium conditions enlarge the intervals of existence. Type III.B equilibrium existence is unaffected.

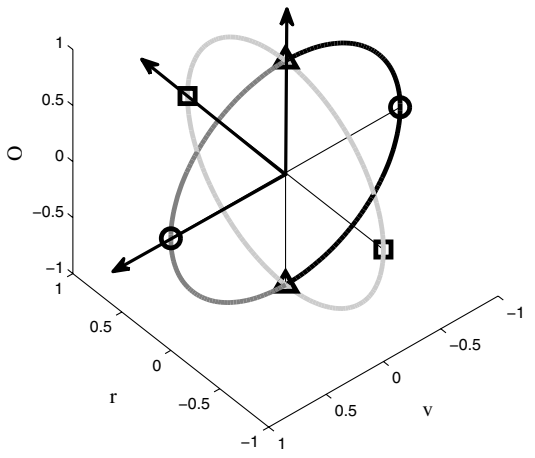

Fig. 3 Equilibria of the sail normal $\hat{n}$ in the LVLH frame L: type I (triangles), type II.A (small circles), type II.B (squares), type III.A.1 (medium gray line), type III.A.2 (black line), and type III.B (light gray line).

Stability of Equilibria

Stability of the equilibria was analyzed in [9] via the Lyapunov function:

$$V = \tfrac{1}{2}{}^L\boldsymbol{\omega}_B \cdot \mathbf{I}_s \cdot {}^L\boldsymbol{\omega}_B + \Psi_a + \Psi_s + \Psi_g + \Psi_x + \tfrac{1}{2}I_n(\omega_s - \omega_{\rm so})^2 - \tfrac{1}{2}{}^A\boldsymbol{\omega}_L \cdot \mathbf{I}_s \cdot {}^A\boldsymbol{\omega}_L + V_o \tag{17}$$

The first term in V is a relative kinetic energy that is zero when the B frame is fixed in L. The Ψ_a, Ψ_s, and Ψ_g terms are potential functions that describe the aerodynamic, solar, and gravity gradient torques as functions of the sail normal $\hat{n}$ attitude as follows:

$$\Psi_a = \tfrac{1}{2}\tau_{\rm am}[1 - \text{sign}\,(\hat{n}\cdot\hat{v})(\hat{n}\cdot\hat{v})^2] \tag{18}$$

$$\Psi_s = \tfrac{1}{2}\tau_{\rm sm}[1 - \text{sign}\,(\hat{n}\cdot\hat{s})(\hat{n}\cdot\hat{s})^2] \tag{19}$$

$$\Psi_g = \tfrac{3}{2}\omega_o^2[(I_n - I_T)(\hat{r}\cdot\hat{n})^2 + I_T] \tag{20}$$

Ψ_x and the quadratic term in ${}^A\boldsymbol{\omega}_L$ are extra terms needed to account for the noninertial reference for the kinetic energy in V_1. Ψ_x is chosen to cancel a particular term in the derivative of V:

$$\Psi_x = -\omega_o \omega_{\rm so} I_n \hat{o}\cdot\hat{n} \tag{21}$$

The environmental torques in Eqs. (10–12) are obtained from Eqs. (18–20), respectively, via

$$\boldsymbol{\tau}_a = \frac{\partial\Psi_a}{\partial\hat{n}} \times \hat{n}, \qquad \boldsymbol{\tau}_s = \frac{\partial\Psi_s}{\partial\hat{n}} \times \hat{n}, \qquad \boldsymbol{\tau}_g = \frac{\partial\Psi_g}{\partial\hat{n}} \times \hat{n} \tag{22}$$

With the total torque $\boldsymbol{\tau} = \boldsymbol{\tau}_a + \boldsymbol{\tau}_s + \boldsymbol{\tau}_g + \boldsymbol{\tau}_c$ including a control torque $\boldsymbol{\tau}_c$, the results are

$$\frac{\mathrm{d}}{\mathrm{d}t}V = {}^L\boldsymbol{\omega}_B \cdot \boldsymbol{\tau}_c \tag{23}$$

Hence, with zero control torque, V is a constant of the motion under the solar, aerodynamic, and gravity gradient torques. Then, if V is a positive definite function of ${}^L\boldsymbol{\omega}_B$ and deviations of $\hat{n}$ are from $\hat{n}_o$ in a neighborhood of $\mathbf{0}$ and $\hat{n}_o$, respectively, then the equilibrium in L is Lyapunov stable [20]. Because $\mathbf{I}_s$ is positive definite, the kinetic term in Eq. (17) is a positive definite function of ${}^L\boldsymbol{\omega}_B$, so that the only question is whether the potential terms in Eq. (17) are positive definite in deviations of $\hat{n}$ from $\hat{n}_o$.

It can be shown [9] that the type I.A equilibria, characterized by $\beta = 0$ (orbit-normal pointing for $\hat{n}$), are stable when

$$-\tau_{\rm am} + \tau_{\rm sm} - \omega_o^2 I_T + \omega_{\rm no}\omega_o I_n > 0 \tag{24}$$

Hence, a large enough spin ω_{no} stabilizes this equilibrium for any orbit altitude, any oblate mass properties ($I_n \geq I_T$, because $\tau_{gm} \geq 0$ is assumed), and any aerodynamic and solar torque magnitudes.

A similar argument for the type I.B equilibrium leads to the sufficient condition:

$$-\tau_{\rm am} - \tau_{\rm sm} - \omega_o^2 I_T - \omega_{\rm no}\omega_o I_n > 0 \tag{25}$$

for Lyapunov stability. Here, a sufficiently negative (retrograde) spin ω_{no} ensures stability. A spinning solar sail operating in the neighborhood of a type I equilibrium was considered in [7], although

no aerodynamic forces were included. The solar torques were also considered constant in the body frame, independent of attitude, so that stability of this equilibrium could not be investigated.

For the type II equilibria, the same approach was used [9], except that these require that $\omega_{no} = 0$ at equilibrium. The sufficient conditions for Lyapunov stability are as follows.

For the type II.A.1 (velocity pointing of $\hat{n}_o$),

$$\tau_{\text{am}} - \tau_{\text{sm}} + \omega_o^2 I_T > 0 \qquad \text{and} \qquad \tau_{\text{am}} + 3\tau_{\text{gm}} > 0 \tag{26}$$

For the type II.A.2 (antivelocity pointing of $\hat{n}_o$),

$$-\tau_{\text{am}} - \tau_{\text{sm}} + \omega_o^2 I_T > 0 \qquad \text{and} \qquad -\tau_{\text{am}} + 3\tau_{\text{gm}} > 0 \tag{27}$$

For the type II.B (nadir or antinadir pointing of $\hat{n}_o$),

$$-\tau_{\text{sm}} - 3\tau_{\text{gm}} + \omega_o^2 I_T > 0 \qquad \text{and} \qquad -\tau_{\text{am}} - 3\tau_{\text{gm}} > 0 \tag{28}$$

Note that Eq. (28) cannot be satisfied, and Eqs. (26) and (27) are affected oppositely by aerodynamic drag but are both destabilized by sufficiently large solar torque.

The same approach can be taken for type III equilibria, resulting in the following stability conditions.

For type III.A.1 ($\phi = 0$),

$$-\tau_{\text{sm}} \operatorname{sign}[\cos(\beta)] + \omega_o^2 I_T > 0 \qquad \text{and} \qquad \tau_{\text{am}} + 3\tau_{\text{gm}} > 0 \tag{29}$$

For type III.A.2 ($\phi = \pi$),

$$-\tau_{\text{am}} - \tau_{\text{sm}} \operatorname{sign}[\cos(\beta)] + \omega_o^2 I_T > 0 \qquad \text{and} \qquad -\tau_{\text{am}} + 3\tau_{\text{gm}} > 0 \tag{30}$$

For type III.B [$\cos(\phi) = 0$],

$$-\tau_{\text{sm}} - 3\tau_{\text{gm}} + \omega_o^2 I_T > 0 \qquad \text{and} \qquad -\tau_{\text{am}} - 3\tau_{\text{gm}} > 0 \tag{31}$$

Note that Eq. (31) cannot be satisfied, and Eqs. (29) and (30) are again oppositely affected by aerodynamic torque. It is interesting to note that the solar torque is destabilizing for equilibria where $\cos\beta > 0$, but it is stabilizing for $\cos\beta < 0$. Aerodynamic torque is destabilizing, except for type III.A.1 and type II.A.1 equilibria.

Because Eqs. (24–31) are only sufficient conditions for stability, failure does not imply instability. In the next section, magnetic damping control is applied to obtain asymptotic stability of the (neutrally) stable equilibria found previously. The addition of a control potential term is also discussed, which enables stabilization of unstable equilibria in some cases.

Magnetic Control

To keep the sailcraft as simple and low cost as possible, a magnetic control approach is considered. This only requires a magnetometer and a sun sensor for attitude determination and B-field measurement and simple wire coils for generating control moments. By controlling current in three orthogonal coils, an arbitrary magnetic moment vector $\boldsymbol{M}_c$ can be created. The resulting control torque on the sailcraft is given by

$$\boldsymbol{\tau}_c = \boldsymbol{M}_c \times \mathbf{B} \tag{32}$$

which shows that the torque is constrained to the plane orthogonal to the local $\mathbf{B}$ vector.

Spin Control

When $\mathbf{B}$ is orthogonal to $\hat{n}$, specifying a magnetic moment in the plane orthogonal to $\hat{n}$ produces torque along $\hat{n}$, allowing spin control to be decoupled from sail normal pointing control [see Eq. (5)]. However, for $\mathbf{B}$ otherwise, magnetic torque cannot be constrained to affect spin only. Here, we maintain approximate decoupling by enabling spin control only when $\mathbf{B}$ is within a specified tolerance of being orthogonal to $\hat{n}$. This produces only intermittent spin control, but it may be adequate for many applications because the environmental disturbances to spin are small (e.g., due to eddy current damping and dissipative solar torques from sail shape variations). When enabled, the spin control law produces magnetic moments in the plane normal to $\hat{n}$:

$$\boldsymbol{M}_{cs} = \frac{k_s(\omega_{\text{no}} - \omega_n)}{|\mathbf{B}|}\hat{\mathbf{B}} \times \hat{n} \tag{33}$$

producing the torque

$$\boldsymbol{\tau}_{cs} = k_s(\omega_{\text{no}} - \omega_n)(\mathbf{I} - \hat{\mathbf{B}}\,\hat{\mathbf{B}}) \cdot \hat{n} \tag{34}$$

Pointing Control

The available magnetic torque can also be constrained to the plane transverse to the sail normal by constraining the magnetic moment to lie along the sail normal. Set

$$\boldsymbol{M}_{cp} = m_p \hat{n} \tag{35}$$

then

$$\boldsymbol{\tau}_{cp} = m_p(\hat{n} \times \mathbf{B}) \tag{36}$$

Thus, magnetic control torque to point the sail normal (and not affect spin rate) must be specified through the scalar control m_p.

B-Dot Damping

The standard B-dot control law [21] generates a vector magnetic moment $\boldsymbol{M}_c$ on the sailcraft by coil current in three orthogonal coils according to

$$\boldsymbol{M}_c = -\frac{k_d}{|\mathbf{B}|^2}\left(\frac{{}^C\mathrm{d}}{\mathrm{d}t}\mathbf{B}\right) \tag{37}$$

This does not require attitude or orbit determination, only a measurement of the rate of change of magnetometer measurements $\mathbf{B}$ in the body frame C. This is often used for spacecraft detumbling after release from the launch vehicle, in which initial rates are much larger than the twice-per-orbit rotation of the B-field (assuming a polar orbit). However, the B-field has a fundamental component that has an approximate period in LVLH of once per orbit, and this control law tends to cause the sailcraft to tumble in LVLH at the same rate. Instead, consider a relative B-dot law referenced to the frame L as follows:

$$\boldsymbol{M}_c = -\frac{k_d}{|\mathbf{B}|^2}\left(\frac{{}^C\mathrm{d}}{\mathrm{d}t}\mathbf{B} - \frac{{}^L\mathrm{d}}{\mathrm{d}t}\mathbf{B}\right) \tag{38}$$

where $\frac{{}^L\mathrm{d}}{\mathrm{d}t}\mathbf{B}$ is obtained from a model of the B-field that would be observed in the L frame. Note, Eq. (38) requires orbit determination to calculate the B-field rate of change in L from the model, and it requires attitude determination to enable the resulting magnetic moment component to be resolved into the body frame C to subtract from magnetometer measurements. To ensure that the torque is not provided along the sail normal, so that ω_n remains constant, we should restrict the magnetic moment to the $\hat{n}$ direction. This would produce

$$\boldsymbol{\tau}_c = -k_d[{}^L\boldsymbol{\omega}_B \cdot (\hat{n} \times \hat{\mathbf{B}})]\hat{n} \times \hat{\mathbf{B}} \tag{39}$$

When used in Eq. (23)

$$\frac{\mathrm{d}}{\mathrm{d}t}V = -k_d|\hat{n} \cdot ({}^L\boldsymbol{\omega}_B \times \hat{\mathbf{B}})|^2 \tag{40}$$

Because the system is not autonomous, due to the time variation of $\hat{\mathbf{B}}$, the LaSalle arguments for asymptotic stability of [9] cannot be applied. Instead, we use a Barbalat [20] argument as follows. The potential terms in Eq. (17) are bounded a priori, and the kinetic term is positive definite, so that V is bounded below. Equation (40) implies that V is monotone decreasing, hence ${}^L\boldsymbol{\omega}_B$ is bounded and V

converges, and by Eq. (39), $\boldsymbol{\tau}_c$ is bounded. From Eq. (4), because ω_n is constant, $\frac{\mathrm{d}}{\mathrm{d}t}\boldsymbol{\omega}_T$ is bounded, hence $\boldsymbol{\omega}_T$ is uniformly continuous, as is ${}^L\boldsymbol{\omega}_B$. Then $\frac{\mathrm{d}}{\mathrm{d}t}V$ is also uniformly continuous, hence by the Barbalat lemma $\frac{\mathrm{d}}{\mathrm{d}t}V \to 0$. This implies that either ${}^L\boldsymbol{\omega}_B \times \hat{\mathbf{B}}$ becomes orthogonal to $\hat{n}$, ${}^L\boldsymbol{\omega}_B$ becomes colinear with $\hat{\mathbf{B}}$, or ${}^L\boldsymbol{\omega}_B \to 0$. Because ${}^L\boldsymbol{\omega}_B$ is always orthogonal to $\hat{n}$, the first requires that $\hat{\mathbf{B}}$ becomes aligned with $\hat{n}$. Although this may approximately occur under the standard B-dot law, it cannot occur with the L-relative B-dot control because, from Eq. (39), this produces zero control torque, and the uncontrolled dynamics (subject only to environmental torques) could not be naturally synchronized with the motion of the independent $\hat{\mathbf{B}}$ field. Likewise, the second option is impossible, because control torque is zero if ${}^L\boldsymbol{\omega}_B$ becomes colinear with $\hat{\mathbf{B}}$. Therefore, ${}^L\boldsymbol{\omega}_B \to \bar{0}$. Because ${}^L\boldsymbol{\omega}_B = 0$ and $\boldsymbol{\tau}_c = 0$ only at equilibria in L, the system state converges to an equilibrium. For a given ω_n, there are at most 10 equilibria from the Equilibrium Spin section, each with a corresponding value of V_i of V. At any such equilibrium, if the potential portion of V is positive definite in deviations δ_n about the equilibrium (sufficient for Lyapunov stability in the Stability of Equilibria section), then there exists an $\epsilon > 0$ and a compact set Ω containing this equilibrium such that $V_i \le V \le V_i + \epsilon$ on Ω, and Ω does not contain any other equilibria. Because V is monotone decreasing, Ω is positively invariant, and the equilibrium contained in this set is asymptotically stable. On the other hand, if the stability conditions in the Stability of Equilibria section fail to hold for an equilibrium, so that the potential portion of V has points arbitrarily close to the equilibrium where $V < V_i$, then beginning at such an orientation with ${}^L\boldsymbol{\omega}_B = \bar{0}$, the state converges to an equilibrium that must be different than the one in question (because V cannot increase) so that equilibrium is unstable. Hence, the use of a B-dot law relative to L produces damping that renders stable equilibria from the Stability of Equilibria section asymptotically stable, and all others unstable. Unfortunately, it does not provide any potential (i.e., orientation dependent) torque to stabilize any unstable equilibria in L.

A common stabilization approach in magnetic attitude control is to compute the required potential torque, assuming full authority torques can be generated, then orthogonally project these torques onto the feasible direction $\hat{n} \times \hat{\mathbf{B}}$. Under restrictions on the spacecraft motion speed, averaging theory has been used [22] to show that full authority performance can be recovered in many cases, owing to the rotation of the B-field. The motion restrictions can hold near stable equilibria, but this approach can fail to stabilize unstable equilibria.

The essential problem is that the projection of control torque onto $\hat{n} \times \hat{\mathbf{B}}$ can alter torque direction significantly, resulting in not only lack of control authority, but further destabilization. What is needed is a control law that provides torques that simultaneously lie along the feasible direction yet never destabilize. This may still fail to control pointing in the presence of environmental disturbances, due to lack of sufficient control authority, but these disturbances would be applied to a system with more robust stability properties. This approach is discussed in the next section.

Magnetic Momentum Error Reduction

The sailcraft angular momentum can be written as

$$
\begin{aligned}
{}^A\mathbf{h}_C &= \mathbf{I}_s \cdot {}^A\boldsymbol{\omega}_C = \mathbf{I}_s \cdot ({}^A\boldsymbol{\omega}_L + {}^L\boldsymbol{\omega}_B + {}^B\boldsymbol{\omega}_C) = I_n(\omega_n)\hat{n} \\
&\quad + I_T[\omega_o(\mathbf{I} - \hat{n}\,\hat{n})\hat{o} + {}^L\boldsymbol{\omega}_B]
\end{aligned} \tag{41}
$$

At a desired equilibrium, $\hat{n} = \hat{n}_o$, $\omega_n = \omega_{\mathrm{no}}$, and ${}^L\boldsymbol{\omega}_B = \bar{0}$, yielding the desired angular momentum:

$$
{}^A\mathbf{h}_{Co} = I_n(\omega_{\mathrm{no}})\hat{n} + I_T\omega_o(\mathbf{I} - \hat{n}\,\hat{n}) \cdot \hat{o} \tag{42}
$$

When torques are transverse to $\hat{n}$, ω_n is constant at ω_{no}, and the angular momentum error relative to the desired equilibrium in L is then

$$
{}^A\mathbf{h}_C - {}^A\mathbf{h}_{Co} = I_n\omega_{\mathrm{no}}(\hat{n} - \hat{n}_o) + I_T{}^L\boldsymbol{\omega}_B + I_T\omega_o(\hat{n}_o\hat{n}_o - \hat{n}\,\hat{n}) \cdot \hat{o} \tag{43}
$$

Collecting terms and defining the constant ω_r by

$$
\omega_r = \tfrac{I_n}{I_T}\omega_{\mathrm{no}} - \omega_o(\hat{n}_o \cdot \hat{o}) \tag{44}
$$

we arrive at the simplified form

$$
{}^A\mathbf{h}_C - {}^A\mathbf{h}_{Co} = I_T\omega_r(\hat{n} - \hat{n}_o) + I_T{}^L\boldsymbol{\omega}_B + \omega_o I_T[(\hat{n}_o - \hat{n}) \cdot \hat{o}]\hat{n} \tag{45}
$$

Consider a Lyapunov function formed from this angular momentum error:

$$
V_h = \tfrac{1}{2}({}^A\mathbf{h}_C - {}^A\mathbf{h}_{Co}) \cdot ({}^A\mathbf{h}_C - {}^A\mathbf{h}_{Co}) \tag{46}
$$

Except for the case where $\hat{n} - \hat{n}_o$ is colinear with ${}^L\boldsymbol{\omega}_B$, this is a positive definite function of $\hat{n} - \hat{n}_o$ and ${}^L\boldsymbol{\omega}_B$.

Defining τ_o as the net torque on the sailcraft at the equilibrium, we find

$$
\begin{aligned}
\frac{\mathrm{d}}{\mathrm{d}t}V_h &= ({}^A\mathbf{h}_C - {}^A\mathbf{h}_{Co}) \cdot \frac{{}^L\mathrm{d}}{\mathrm{d}t}({}^A\mathbf{h}_C - {}^A\mathbf{h}_{Co}) = ({}^A\mathbf{h}_C - {}^A\mathbf{h}_{Co}) \\
&\quad \cdot \left[\frac{{}^A\mathrm{d}}{\mathrm{d}t}({}^A\mathbf{h}_C - {}^A\mathbf{h}_{Co}) - {}^A\boldsymbol{\omega}_L \times ({}^A\mathbf{h}_C - {}^A\mathbf{h}_{Co})\right] \\
&= ({}^A\mathbf{h}_C - {}^A\mathbf{h}_{Co}) \cdot (\tau - \tau_o)
\end{aligned} \tag{47}
$$

At the equilibrium, no control torque is required, so that τ_o consists only of environmental torques, which are transverse to $\hat{n}$ from Eq. (22). Likewise, $\tau = \tau_c + \tau_e$ is transverse to $\hat{n}$ when the control torques τ_c are. Then, using Eq. (45), we obtain

$$
\tfrac{\mathrm{d}}{\mathrm{d}t}V_h = [I_T\omega_r(\hat{n} - \hat{n}_o) + I_T{}^L\boldsymbol{\omega}_B] \cdot (\tau_c + \tau_e - \tau_o) \tag{48}
$$

Finally, write $\tau_e = \delta\tau_e + \tau_o$ to obtain

$$
\tfrac{\mathrm{d}}{\mathrm{d}t}V_h = [I_T\omega_r(\hat{n} - \hat{n}_o) + I_T{}^L\boldsymbol{\omega}_B] \cdot (\tau_c + \delta\tau_e) \tag{49}
$$

Feasible magnetic torque is in the form $\tau_c = m_p(\hat{n} \times \hat{\mathbf{B}})$, and so we choose the scalar magnetic moment:

$$
m_p = -k[\omega_r(\hat{n} - \hat{n}_o) + {}^L\boldsymbol{\omega}_B] \cdot (\hat{n} \times \hat{\mathbf{B}}) \tag{50}
$$

for some positive gain k. Then, in the absence of environmental torque deviations $\delta\tau_e$ from the equilibrium torque τ_o, we have

$$
\tfrac{\mathrm{d}}{\mathrm{d}t}V_h = -kI_T\{[\omega_r(\hat{n} - \hat{n}_o) + {}^L\boldsymbol{\omega}_B] \cdot (\hat{n} \times \hat{\mathbf{B}})\}^2 \tag{51}
$$

showing that angular momentum error cannot be increased by the magnetic control law (50). The presence of environmental torque deviations $\delta\tau_e$ may cause angular momentum error increase if the contraction caused by the control is weak (i.e., if $\hat{n} \times \hat{\mathbf{B}}$ is nearly orthogonal to $\omega_r(\hat{n} - \hat{n}_o) + {}^L\boldsymbol{\omega}_B$ or if $\hat{n}$ is nearly colinear to $\hat{\mathbf{B}}$). On the other hand, if these occurrences are rare, and k is large enough, the persistent decrease in V_h caused by the control can be expected to dominate the occasional increase caused by the disturbances $\delta\tau_e$.

Note that the control law (50) produces a damping torque proportional to that provided by the relative B-dot control law (39), but it also provides a torque dependent on the orientation error $\hat{n} - \hat{n}_o$. This stabilizing potential, although time varying with the B-field, raises the possibility that the destabilizing environmental deviations $\delta\tau_e$ might be overcome. Control performance in the presence of these disturbances is evaluated in the Simulations section.

It is interesting to observe that the momentum error reduction control law can be implemented as a relative B-dot law, provided that the reference spin rate is suitably specified. Instead of the B-dot law relative to L in Eq. (39), consider B-dot relative to a frame R that has one axis aligned with $\hat{n}_o$ but has a spin rate ω_{sr} about $\hat{n}_o$ relative to L. Then, the magnetic moment

$$\boldsymbol{M}_c = -\frac{k_d}{|\mathbf{B}|^2}\left[\hat{n}\cdot\left(\frac{^C\mathrm{d}}{\mathrm{d}t}\mathbf{B} - \frac{^R\mathrm{d}}{\mathrm{d}t}\mathbf{B}\right)\right]\hat{n} = \frac{k_d}{|\mathbf{B}|^2}[\hat{n}\cdot(^R\boldsymbol{\omega}_C \times \mathbf{B})]\hat{n}$$
$$= \frac{k_d}{|\mathbf{B}|^2}\{\hat{n}\cdot[(^L\boldsymbol{\omega}_B + {}^B\boldsymbol{\omega}_C - {}^L\boldsymbol{\omega}_R)\times\mathbf{B}]\}\hat{n} = \frac{k_d}{|\mathbf{B}|^2}\{\hat{n}\cdot[(^L\boldsymbol{\omega}_B$$
$$+ \omega_s\hat{n} - \omega_{sr}\hat{n}_o)\times\mathbf{B}]\}\hat{n} = -\frac{k_d}{|\mathbf{B}|^2}[^L\boldsymbol{\omega}_B\cdot(\hat{n}\times\mathbf{B})]\hat{n}$$
$$-\frac{k_d}{|\mathbf{B}|^2}\omega_{sr}[\mathbf{B}\cdot(\hat{n}\times\hat{n}_o)]\hat{n} \tag{52}$$

produces the control torque

$$\boldsymbol{\tau}_c = -k_d{}^L\boldsymbol{\omega}_B\cdot(\hat{n}\times\hat{\mathbf{B}})(\hat{n}\times\hat{\mathbf{B}}) - k_d\omega_{sr}\hat{\mathbf{B}}\cdot(\hat{n}\times\hat{n}_o)(\hat{n}\times\hat{\mathbf{B}}) \tag{53}$$

Noting that $\hat{\mathbf{B}}\cdot(\hat{n}\times\hat{n}_o) = (\hat{n}-\hat{n}_o)\cdot(\hat{n}\times\hat{\mathbf{B}})$, Eq. (53) is equivalent to Eq. (50) by choosing $k_d = k$ and $\omega_{sr} = \omega_r$.

Simulations

As a design reference, a 3U CubeSat [23] standard architecture will be used for the CubeSat solar sail spacecraft (CubeSail), for which the mission objective is to demonstrate solar sail technology to enable the development of similar solar sail propelled spacecraft to perform a future mission to study Earth's geomagnetic tail. CubeSail mission requirements are to stow and deploy the sailcraft from a standard poly picosatellite orbital deployer [24], deploy the sailcraft to a stable operational state, control the attitude of the sail, demonstrate characteristic acceleration greater than 0.11 mm/s^2, and maintain an operational state for longer than 30 days. To meet these objectives, derived requirements for the sail subsystem are a total of 1.7 kg mass, with a square flat sail membrane with a 40 m^2 area. The sail is folded and rolled around a central spine to fit within a 2U CubeSat outline, and it is deployed by stored elastic energy in four booms located along the diagonals of the square sail. The CubeSail bus is packaged within a 1U CubeSat module (with a mass of 1.3 kg) located on the supporting spine, such that the sailcraft CM is offset by $r_c = 9.5$ cm from the deployed sail plane along the sail normal $\hat{n}$. In the stowed configuration, the sailcraft is prolate, with principal moments of inertial $I_n = 0.005$ and $I_T = 0.025$ kg $\cdot$ m^2. In the deployed state, the sailcraft is oblate, with $I_n = 11.335$ and $I_T = 5.703$ kg $\cdot$ m^2. The CubeSail orbit baseline is a dawn–dusk sun-synchronous orbit at 700 km altitude, with a dawn–dusk orientation of orbit nodes. Mean atmospheric density for this altitude [16] was assumed. For the purposes of the simulations, the 700 km altitude circular polar orbit is employed only as a baseline, and variations are considered to investigate the effects on control robustness.

The baseline avionics subsystem consists of a Pumpkin, Inc. FM430 RISC microcontroller board using the salvo real-time operating system running custom CubeSail C code, a MicroHard MHX2420 2.4 GHz modem for communications, and four spring-loaded solar panels that hinge from the front edge of the CubeSail bus to cant at 45 deg to the sail normal. Six gallium–arsenide cells are used per panel (at 2.2 V/cell) for power generation, and power conditioning is provided by a custom board designed by SpaceQuest, including three lithium–ion battery cells (3.6 V/cell). The attitude determination and control system employs a Honeywell HMR2300 triaxial magnetometer, a SpaceQuest SS-440 two axis digital sun sensor, a modified SpaceQuest GPS-12-V1 global positioning system unit, and three custom-wound magnetic torque coils on three orthogonal faces of the CubeSail bus, with 300 turns of 27 American wire gauge copper wire each. Sail imaging is accomplished with four STMicro VS6724 pinhole cameras pointed toward the sail plane through ports in four faces of the bus. Preliminary assessments indicate that imaging, attitude determination, communications, and processing will require a total peak power of under 2 W. Magnetic attitude control can produce a peak magnetic moment of 1.4 A $\cdot$ m^2 with this design, requiring 6 W. Each solar panel generates 3.4 W at a solar beta angle of 45 deg, for a total average available power of 13.6 W. Except for one mission mode (sail imaging mode), the 1.4 A $\cdot$ m^2 limit on the magnetic moment and 8 W total power is sufficient for all phases of the mission, and this is available from the solar arrays with considerable margin.

A multisegment mission scenario was evaluated in simulation, beginning with a detumble segment in which a standard B-dot law was employed to dissipate initial angular momentum from launch vehicle tip off before deploying the sail. A sail imaging mode was then acquired, after sail deployment, in which the sail was pointed toward the ground (using a type III.B equilibrium), for validation of the deployed sail shape from both an onboard camera and ground telescopes. The next phase was parking mode acquisition (a type I.A equilibrium), which serves as a safe mode requiring no attitude or orbit determination and points solar arrays at the sun to charge sailcraft batteries. An orbit-raising type III.A.2 equilibrium was then acquired to validate the characteristic acceleration capability of the sail. Finally, a deorbit mode was entered by pointing to a type III.A.1 equilibrium.

Detumble Mode

The standard B-dot control law (37) was used to detumble the spacecraft after a launch vehicle tip off with the sail undeployed. Here, the sailcraft is a 10 by 10 by 30 cm box, in which a 2 cm CP–CM offset is assumed. An initial tumble rate of 5 deg/s was assumed, in a random direction, and a B-dot gain $k_d = 10$ N $\cdot$ m $\cdot$ s/rad was used in Eq. (37). Figure 4 shows the resulting evolution of cone and clock angles, using the MATLAB® ODE113 integrator, producing an antinadir pointing orientation of $\hat{n}$ ($\beta = 90$ deg and $\phi = -90$ deg) after about five orbits, with 0.025 A $\cdot$ m^2 peak magnetic moment. Nadir pointing is also possible, depending on which gravity gradient hemisphere captures the sail normal. Smaller gains prolong the detumble interval, and larger gains tend to lock the sailcraft to the B-field rotation, resulting in a once-per-orbit rotation of $\hat{n}$ in L. The advantage of this control law is that neither orbit nor attitude determination are required for implementation, only magnetometer measurements, which are time multiplexed with torque coil activation.

Sail Imaging Mode

Once the sail is deployed, the nadir or antinadir pointing equilibria are unstable. In fact, from the Stability of Equilibria section, all type III.B equilibria are unstable with the sail deployed. Although the sail could be viewed from the ground in type I or type III.A equilibria, the sail is edge-on to the Earth, so that ground viewing would require

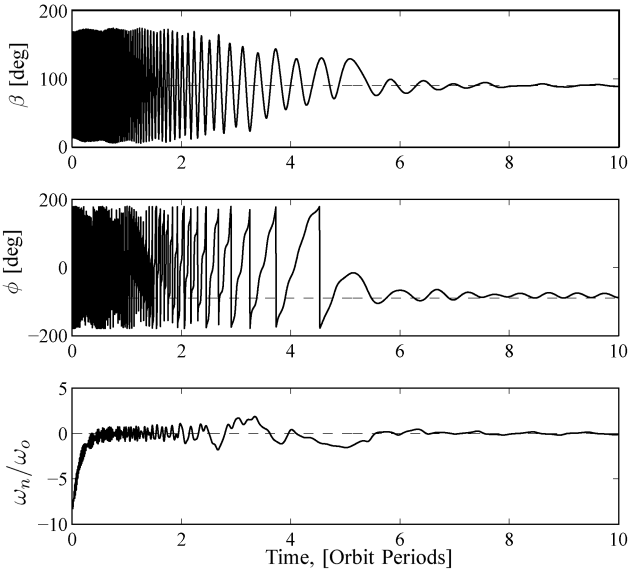

Fig. 4 Detumble behavior using a standard B-dot control law (37) with a gain of $k_d = 10$ N $\cdot$ m $\cdot$ s/rad and an initial tipoff rate of 5 deg/s (sail undeployed).

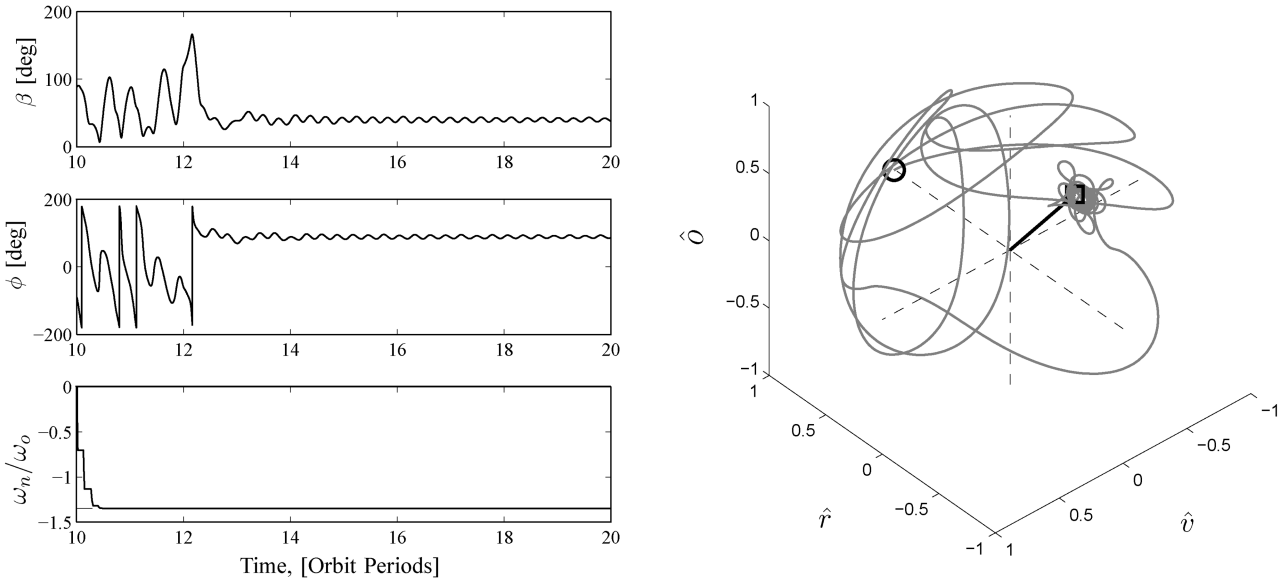

Fig. 5 Simulation of the B-dot damping control and spin control for ground viewing mode.

a cross track location of several hundred kilometers, increasing the slant range considerably. Instead, magnetic control can be applied to stabilize at a type III.B equilibria, in which the sail can be viewed from a closer location on the ground. Pointing in this mode requires a stabilizing potential that can dominate the destabilizing environmental potentials. Here, we use the momentum error reduction control law, implemented as the relative B-dot law (53), with the gain $k_d = 100$ N · m · s/rad and the reference spin rate $\omega_{sr} = -3.45\omega_o$ to point at a cone angle $\beta = 40$ deg and a clock angle $\phi = 90$ deg. Spin control is also enabled, as previously, with a gain $k_s = 100$ N · m · s/rad and a desired inertial spin rate $\omega_{\text{no}} = -1.35\omega_o$ (see Fig. 5). The naturally unstable type III.B equilibrium at $\beta = 40$ deg and $\phi = 90$ deg is stabilized by damping and potential torques from a relative B-dot control law. Desired spin rate is $\omega_{no} = -1.35\omega_o$. Simulation begins (circle) at the end of the detumble segment and converges to the equilibrium (square) in approximately three orbits. Peak magnetic moments are clamped at 5.0 A · m^2, which is achieved at several points during the transition. Although magnetic control does work in this case, stability is rather tenuous (β angles larger than 45 deg do not work) and large gains and magnetic control moments are required.

Parking Mode

Checking the intervals of equilibrium existence from the Equilibrium Spin section and their stability from the Stability of Equilibria section, it can be seen that for this sailcraft and this orbit, a spin rate ω_n larger than $0.72\omega_o$ permits only two equilibria in L. Both are type I: one with $\hat{n}$ aligned with orbit normal $\hat{o}$ and the other aligned with $-\hat{o}$. Only the former is stable, making it essentially globally asymptotically stable with the addition of damping control torque [9]. Orbit-normal pointing with suitable spin is therefore a good candidate for a safe parking mode, which can be maintained with low power and minimal control complexity and provides direct sun pointing for battery charging. Here, we use the same B-dot law as in the detumble phase, with the same gain $k_d = 10$ N · m · s/rad, but with the magnetic moment projected onto the $\hat{n}$ direction to provide damping for asymptotic stability (as discussed in the B-Dot Damping section). In addition, spin control (as discussed in the Spin Control section) with a gain of $k_s = 10$ N · m · s/rad and a desired inertial spin of $\omega_{\text{no}} = \omega_o$ are enabled along with B-dot damping at the start of the parking mode acquisition phase. Figure 6 shows how the sail cone and clock angles and spin velocity propagate in simulation. Simulation begins (circle) at the end of the ground viewing segment

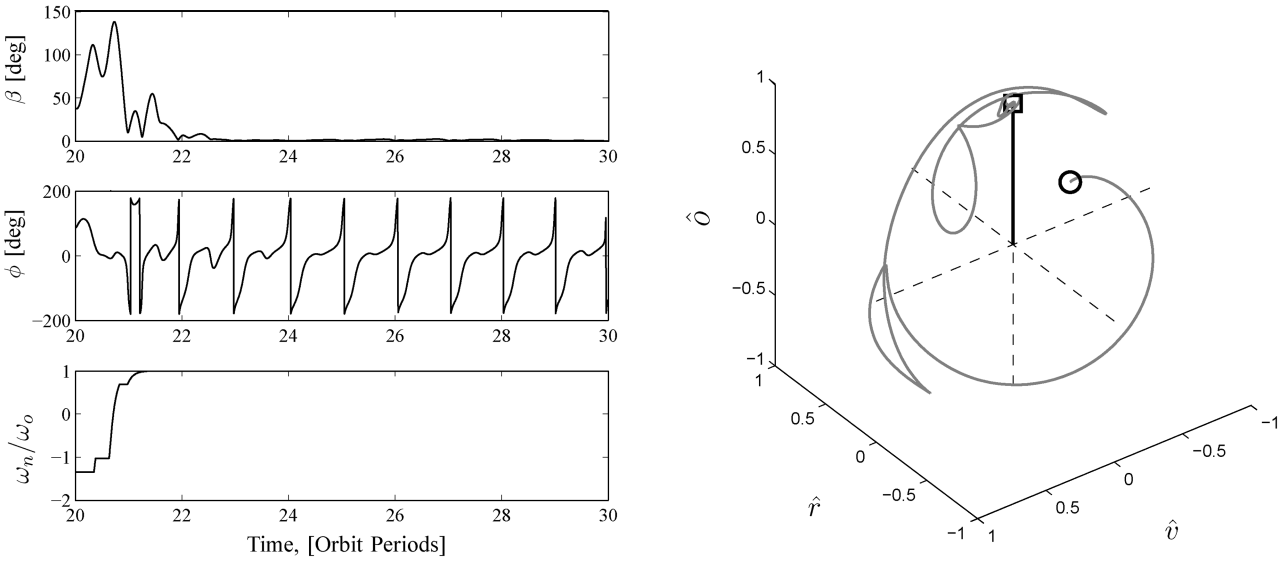

Fig. 6 Simulation of the B-dot damping control and spin control for parking mode at the essentially globally asymptotically stable type I.A equilibrium corresponding to $\omega_{\text{no}}/\omega_o = 1.0$.

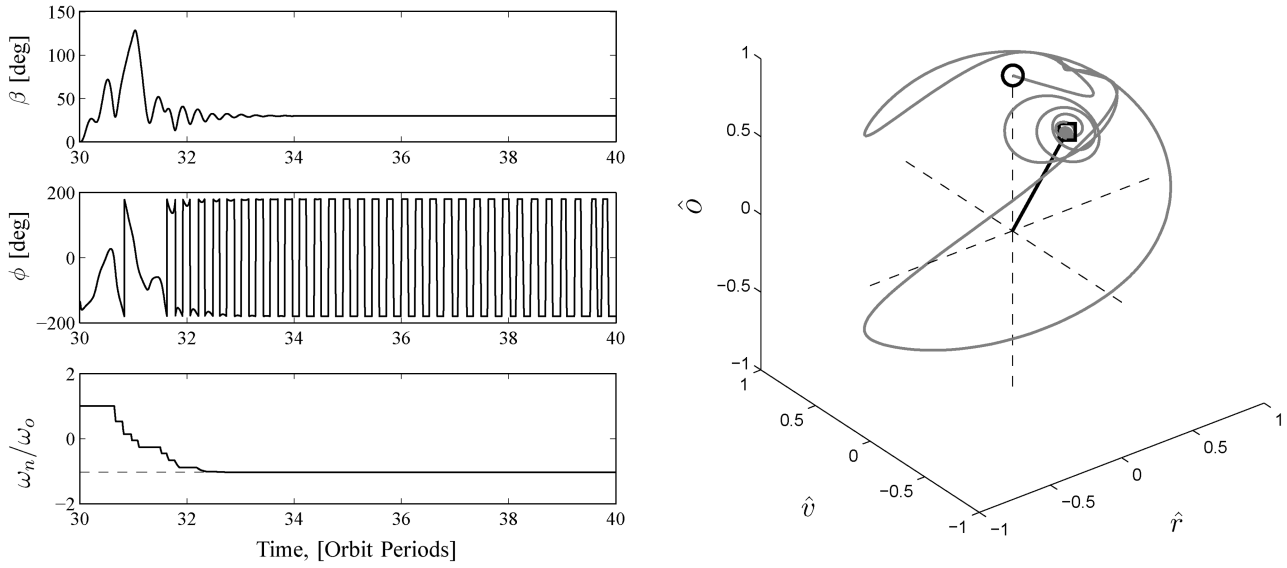

Fig. 7 Simulation of the sail normal $\hat{n}$ propagation in the LVLH frame L toward a type III.A.2 orbit-raising equilibrium.

with the sail deployed and converges to the equilibrium (square) at $\beta = 0$ (where ϕ is irrelevant) in approximately two orbits. The peak magnetic moment is clamped at 0.5 A · m^2, which is achieved at several points during the transition.

Orbit-Raising Mode

A type III.A.2 equilibrium produces orbit-raising solar thrust. Optimum orbit-raising cone angle β depends on sail reflectance properties and on the aerodynamic drag, but it typically occurs for angles in the neighborhood of 30 deg. Although this is an unstable equilibrium, the destabilizing environmental torques are weaker than the case of type III.B equilibria in the ground viewing mode. In particular, gravity gradient is actually stabilizing here, but aerodynamic torques are not. As a result, magnetic control is more effective in this mode. The momentum error reduction control is applied with a gain of $k_d = 10$ N · m · s/rad and $\omega_{sr} = -2.93\omega_o$, along with a spin control gain of $k_s = 10$ N · m · s/rad and $\omega_{\text{no}} = -1.04\omega_o$. Figure 7 shows how this can stabilize the desired orbit-raising equilibrium, beginning (circle) at the end of the parking mode (note the reverse angle view of the L frame). The sail normal $\hat{n}$ converges to $\beta = 30$ deg and $\phi = 180$ deg (square) in approximately two orbits. The damping gains $k_d = 10$ N · m · s/rad and the spin control gains $k_s = 10$ N · m · s/rad. The magnetic control moments are less than 1 A · m^2.

Deorbit Mode

This equilibrium has $\omega_{sr} = \omega_{\text{no}} = 0$ and is naturally stable, hence only damping control is needed. In fact, the potential term in the momentum error reduction control law is zero when $\omega_{sr} = 0$, so that only damping control is provided by that control law. See Fig. 8, in which $\hat{n}$ is attracted to the vicinity of $\beta = 90$ deg and $\phi = 0$ deg (square). The damping gains $k_d = 3$ N · m · s/rad and the spin control gains $k_s = 10$ N · m · s/rad. Peak magnetic moments are less than 0.2 A · m^2.

Magnetic Control Robustness

If the orbit normal $\hat{o}$ is not aligned with the sailcraft-to-sun vector $\hat{s}$, then $\hat{s}$ cones in the L frame at orbit rates, causing a periodic torque that eliminates equilibria in the L frame. However, a sufficiently strong attraction to a desired orientation $\hat{n}_o$ in L, due to the stiffness and damping control laws, makes the system robust to this perturbation torque. Similarly, specifying a desired inertial spin rate ω_{no} that is incorrect for the parameters τ_{am}, τ_{sm}, ω_o, I_n, or I_T causes the desired orientation $\hat{n}_o$ in L to no longer be at an equilibrium. The control law provides continuous torque to offset this disturbance from $\hat{n}_o$ pointing. Figure 9 shows the case of Fig. 7 with a large orbit precession (20 deg in right ascension) of $\hat{o}$ away from sun pointing, and a desired spin rate ω_{no} that is 20% too large in magnitude (e.g., resulting from uncertainty in the mass properties

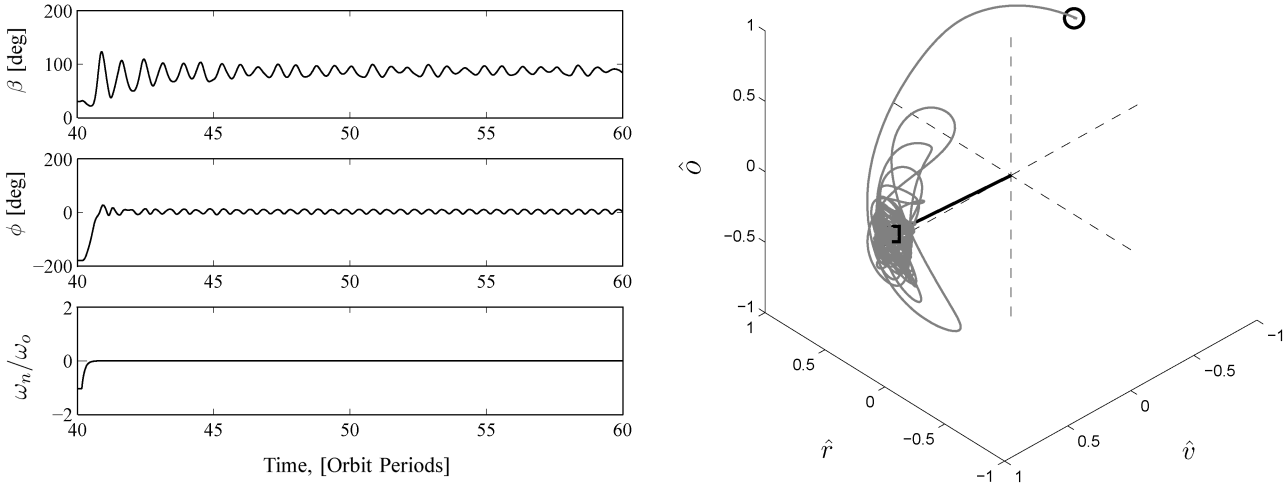

Fig. 8 Deorbit mode, beginning (circle) at the end of the orbit-raising mode.

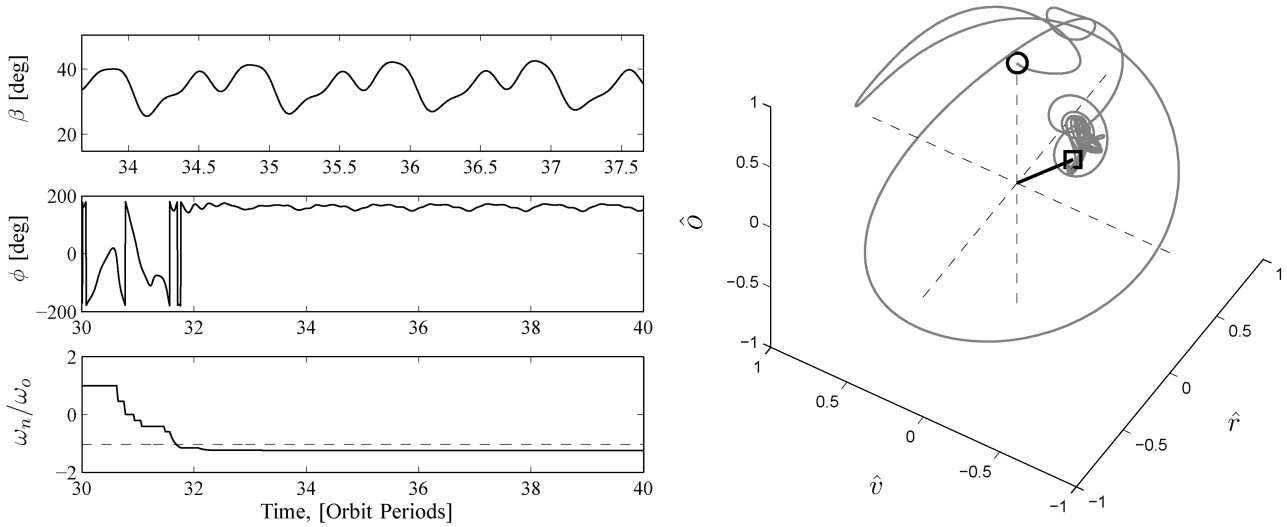

Fig. 9 Propagation $\hat{n}$ in the LVLH frame, in the orbit-raising mode, under perturbations in orbit and spin rate.

or the environmental torques). The view in the L frame is reversed for clarity, and the simulation begins at the end of the parking mode (circle). Motion converges to the close vicinity of the desired orbit-raising attitude in about two orbits, as before, but a steady-state ripple results from these disturbances. The resulting pointing error has a cone angle offset of approximately 4 deg and an orbit-periodic ripple of less than 15 deg, demonstrating robustness of the magnetic control to these perturbations at this naturally unstable equilibrium. The required magnetic moment has a steady-state amplitude of less than $0.5\ \mathrm{A}\cdot\mathrm{m}^2$.

Conclusions

For small satellite applications, the mass and cost associated with attitude control is an especially significant factor in the system design. Although solar sails can provide long-term thrust for orbit changes or orbit maintenance, attitude disturbances can be much larger for solar sails, due to the large area-to-mass ratio for which they are designed. This paper has shown that these environmental torques can be advantageously employed, together with appropriate spin dynamics, such that thrust vector pointing control in various orbit rate coning modes can be achieved for a virtually unlimited duration.

This capability relies on operating the sailcraft near equilibrium points, in which environmental torques balance momentum precession. The complete set of pointing equilibria in the LVLH frame was reviewed, along with its use in various sailcraft operational modes of interest, and the dependence of their existence on orbit and sailcraft parameters. Whereas Lyapunov stability exists for some of these equilibria, many are unstable, and additional control torques are required.

Magnetic control was considered to stabilize sailcraft attitude about desired equilibria in the LVLH frame. A variation on the standard B-dot law was introduced that guarantees that feasible magnetic torques do not destabilize, using a Lyapunov–Barbalat argument based on an angular momentum error formulation. This approach was shown to work in simulations in the presence of environmental torque variations in several operationally useful coning modes, progressing from detumble, to ground viewing, to parking, to orbit-raising, to deorbit modes.

This control approach was also shown to be robust against likely imperfections in sailcraft operation: coning of the sun vector in LVLH and an inaccurate balance between environmental torques and momentum precession, due to inaccurate knowledge of sailcraft/orbit/environmental parameters.

Acknowledgment

Support for this work was provided by the NASA Marshall Space Flight Center (NNX07AO89G) and is gratefully acknowledged.

References

[1] Lawrence, D. A., and Piggott, S., "Integrated Trajectory and Attitude Control for a Four-Vane Solar Sail," AIAA Guidance, Navigation, and Control Conference, AIAA Paper 2005-6082, Aug. 2005.

[2] Rios-Reyes, L., and Scheeres, D., "Robust Solar Sail Trajectory Control for Large Pre-Launch Modeling Errors," AIAA Guidance, Navigation, and Control Conference, AIAA Paper 2005-6173 Aug. 2005.

[3] Lawrence, D. A., Irwin, T. J., and Whorton, M. S., "Solar Sail Thrust Measurement During Coning Operations," AIAA Guidance, Navigation, and Control Conference, AIAA Paper 2006-6183, Aug. 2006.

[4] McInnes, C. R., *Solar Sailing: Technology, Dynamics, and Mission Applications*, Springer–Praxis, New York, pp. 19–25, 47–50, 1999.

[5] Rios-Reyes, L., and Scheeres, D. J., "Solar Sail Navigation: Estimation of Force, Moments, and Optical Parameters," *Journal of Guidance, Control, and Dynamics*, Vol. 30, No. 3, 2007, pp. 660–668. doi:10.2514/1.24340

[6] Bladt, J. J., Lawrence, D. A., and Ward, L. M., "Solar Sail Attitude Control Sensitivity to Solar Radiation Pressure Model Accuracy," AAS/AIAA Space Flight Mechanics Conference, American Astronomical Society Paper 04-282, Feb. 2004.

[7] Wie, B., "Solar Sail Attitude Control and Dynamics: Parts 1 and 2," *Journal of Guidance, Control, and Dynamics*, Vol. 27, No. 4, 2004, pp. 526–544. doi:10.2514/1.11134

[8] Sakamoto, H., Park, K. C., and Miyazaki, Y., "Effect of Static and Dynamic Solar Sail Deformation on Center of Pressure and Thrust Forces," AIAA Guidance, Navigation, and Control Conference, AIAA Paper 2006-6184, Aug. 2006.

[9] Lawrence, D. A., and Whorton, M. S., "Solar Sail Dynamics and Coning Control in Circular Orbits," *Journal of Guidance, Control, and Dynamics*, Vol. 32, No. 3, 2009, pp. 974–985. doi:10.2514/1.35970

[10] Lappas, V., Wokes, S., Leipold, M., Lyngvi, A., and Falkner, P., "Guidance and Control for an Interstellar Heliopause Probe (IHP) Solar Sail Mission to 200 AU," AIAA Guidance, Navigation, and Control Conference, AIAA Paper 2005-6085, Aug. 2005.

[11] Lappas, V., Wie, B., McInnes, C., Tarabini, L., Gomes, L., and Wallace, K., "Microsolar Sails for Earth Magnetotail Monitoring," *Journal of Spacecraft and Rockets*, Vol. 44, No. 4, 2007, pp. 840–848. doi:10.2514/1.23456

[12] Hughes, P. C., *Spacecraft Attitude Dynamics*, Wiley, New York, 1986, pp. 232–264, 354–382.

[13] Kane, T. R., and Levinson, D. A., *Dynamics: Theory and Applications*, McGraw–Hill, New York, 1985, pp. 66–70, 370.

[14] Nakano, T., "A Study on the Stability of Spinning Solar Sailcraft with Huge Membrane," *Proceedings of the 56th International Astronautical Congress of the International Astronautical Federation*, IAC-05-A.4.01, Fukuoka, Japan, Oct. 2005.

[15] Rotunno, M., Basso, M., Pome, A. B., and Sallusti, M., "A Comparison of Robust Attitude Control Techniques for a Solar Sail Spacecraft," AIAA Guidance, Navigation, and Control Conference, AIAA Paper 2005-6083, Aug. 2005.

[16] Wertz, J. R. (ed.), *Spacecraft Attitude Determination and Control*, Kluwer Academic, Dordrecht, The Netherlands, 1978, pp. 566–574.
[17] Thomson, W. T., "Spin Stabilization of Attitude Against Gravity Torque," *Journal of the Astronautical Sciences*, Vol. 9, No. 1, 1962, pp. 31–33.
[18] Pringle, R., "Bounds on the Libration of a Symmetrical Satellite," *AIAA Journal*, Vol. 2, No. 5, 1964, pp. 908–912.
doi:10.2514/3.2436
[19] Likins, P. W., "Stability of a Symmetrical Satellite in Attitudes Fixed in an Orbiting Reference Frame," *Journal of the Astronautical Sciences*, Vol. 12, No. 1, 1965, pp. 18–24.
[20] Khalil, H. K., *Nonlinear Systems*, 3rd ed., Prentice–Hall, Upper Saddle River, NJ, 2002, pp. 114, 128.
[21] Stickler, A. C., and Alfriend, K. T., "Elementary Magnetic Attitude Control System," *Journal of Spacecraft and Rockets*, Vol. 13, No. 5, 1976, pp. 282–287.
doi:10.2514/3.57089
[22] Lovera, M., and Astolfi, A., "Global Magnetic Attitude Control of Spacecraft in the Presence of Gravity Gradient," *IEEE Transactions on Aerospace and Electronic Systems*, Vol. 42, No. 3, July 2006, pp. 796–805.
doi:10.1109/TAES.2006.248214
[23] Lan, W., Brown, J., Torrian, A., Coelho, R., Brooks, L., and Suari, J. P., "CubeSat Development in Education and Into Industry," Space 2006, AIAA Paper 2006-7296, Sept. 2006.
[24] Puig-Suari, J., Turner, C., and Ahlgren, W., "Development of the Standard CubeSat Deployer and a CubeSat Class PicoSatellite," *Proceedings of the IEEE Aerospace Conference*, Vol. 1, IEEE Publications, Piscataway, NJ, March 2001, pp. 347–353.
doi:10.1109/AERO.2001.931726

D. Spencer
Associate Editor